Single-electron transport and magnetic properties of Fe-SiO_2 nanocomposites prepared by ion implantation

Peter Lobotka,* J. Dérer, and I. Vávra
Institute of Electrical Engineering, Slovak Academy of Sciences, Dubravska cesta 9, 84104, Bratislava, Slovakia

C. de Julián Fernández, G. Mattei, and P. Mazzoldi
Dipartimento di Fisica "Galileo Galilei," Università degli Studi di Padova, via F. Marzolo, 8, I-35131 Padova, Italy
(Received 14 July 2006; revised manuscript received 20 October 2006; published 19 January 2007)

The electric transport, magnetic, and magnetotransport properties of Fe-SiO_2 nanocomposites prepared by Fe-ion implantation into silica were investigated. The structural studies revealed bcc Fe nanoparticles of an average size of 3 nm dispersed in a 100-nm-thick nanocomposite layer formed within the silica substrate. Using special thin-film electrodes that were only 100 nm apart, in-plane electrical measurements were performed in a temperature range of 4–300 K. Though no external gate electrode was used, single-electron transport phenomena (Coulomb blockade and Coulomb staircase) were observed at 4 K. The presence of Coulomb steps in *I-V* curves implies that the electric transport was realized by the tunneling of electrons via a random quasi-one-dimensional chain of a few isolated iron nanoparticles. The magnetic properties of the nanoparticles were determined by surface effects and by the superparamagnetic behavior. The nanoparticles exhibited enhanced anisotropy and were dipolarly interacting. However, the tunneling current was found to be independent of external magnetic field; i.e., no tunneling magnetoresistivity (TMR) was measured at 77 K. At this temperature the nanoparticles were superparamagnetic. Presumably, a low volumetric concentration of Fe nanoparticles ($<14\%$) and a spin-flip process due to residual single Fe atoms present in the silica barriers were responsible for the absence of the TMR effect.

DOI: 10.1103/PhysRevB.75.024423 PACS number(s): 73.23.Hk, 73.63.−b, 66.30.Qa, 75.20.−g

I. INTRODUCTION

Nanocomposite materials are studied because of their interesting optical, magnetic, electrical, magneto-optic, catalytic, and other properties. From the point of view of electrical conductivity of the constituents, practically all combinations of materials have been studied so far: metal/insulator, semiconductor/insulator, magnetic/nonmagnetic metals, etc. In particular, if the matrix is an insulator and the metallic nanoparticle concentration is just below the percolation limit, charge transport is accomplished mainly by the tunneling of electrons between the nanoparticles.[1,2] Due to the small size of the nanoparticles, which implies charging energies from several tens to several hundreds of meV, the transport is suppressed by the Coulomb blockade of tunneling,[3] which leads to a threshold voltage in current-voltage (*I-V*) characteristics. When the nanoparticles are ferromagnetic, the nanocomposites show considerable magnetoresistivity because the tunneling of electrons is spin dependent.[4] This effect is called tunneling magnetoresistivity (TMR), and it has been explained in general terms by Julliere[5] and extensively investigated in ferromagnetic metal-insulator-metal tunnel junctions.[6] The TMR should depend critically on the magnetic properties of the nanoparticles, which are size dependent.[7–9] In particular, the superparamagnetic effect determines the enhanced and temperature-dependent misalignment of the relative orientation of the nanoparticle magnetizations at zero magnetic field, which leads to enhanced electrical resistance. The superparamagnetic behavior occurs at temperatures above the so-called blocking temperature T_B, where irreversible processes, such as hysteresis, disappear because the thermally driven demagnetization energy is larger than the energy responsible for the irreversible process. This energy is proportional to the particle size and the magnetic anisotropy of the nanoparticle (its size dependence being a consequence of the surface anisotropy). All that implies that both the magnetic and transport properties are critically dependent on the composite nanostructure.

Several techniques are used for the preparation of this kind of nanocomposite: e.g., sputtering from a composite target,[10] sequential sputtering,[11,12] laser ablation,[13] plasma jet,[14] ion implantation,[15–18] and others. The selection of a proper deposition technique must take into account the achievable quality of the deposited tunneling barrier [represented by several nm thick insulator (matrix) between the adjacent ferromagnetic nanoparticles] because any impurity present in the barrier could cause a spin flip and thus decrease the TMR value. Another important parameter is the average interparticle distance that should be typically about 2–3 nm to ensure sufficiently high tunneling current.

Ion implantation technique is a well-established procedure to obtain nanocomposites of a wide range of metals and insulators.[19–21] This technique allows one to obtain well-controlled nanostructures by choosing proper implantation conditions and successive thermal treatment. From this point of view, one of the best results concerning magnetotransport was obtained in a Fe-Al_2O_3 nanocomposite, prepared by metal implantation into a single-crystalline substrate, its successive annealing aiming mainly at recovering the single crystallinity of the matrix.[16]

Here we report the electrical and magnetic properties of a Fe-SiO_2 nanocomposite prepared by ion implantation of Fe into silica glass. One of the aims of this work was to mini-

mize the volume of the ion-implanted nanocomposites probed by dc current. Therefore, by using optical photolithography and electromigration, thin-film gold planar electrodes were patterned on top of the nanocomposite that were less than 100 nm apart. Though no external gate electrode was patterned, we succeeded in the observation of single-electron transport phenomena: a Coulomb blockade (CB) and Coulomb staircase (CS) in *I-V* characteristics. Nevertheless, no negative tunneling magnetoresistivity was found at 77 K. The magnetic properties of the nanocomposites were studied to elucidate the absence of TMR.

II. EXPERIMENTAL

A. Sample preparation and characterization

The samples were prepared by implanting fused silica glass slides (Hereaus) with 15×10^{16} Fe^+/cm^2 at 180 keV using a DANFYSIK 200-keV ion implantation apparatus at INFN National Laboratories Legnaro (Italy). The current density was maintained below 2 $\mu A/cm^2$ in order to avoid heating of the sample during the implantation process.

Structural studies were realized at CNR-IMM Laboratories in Bologna (Italy) using a field-emission FEI TECNAI F20 SuperTwin FEG(S) transmission electron microscope (TEM) operating at 200 kV and equipped with a EDAX energy-dispersive x-ray spectrometer (EDS). Selected-area electron diffraction (SAED) was used to determine the structure of the nanoparticles. In addition, grazing-incidence x-ray diffraction (GIXRD) studies were realized in a parallel-beam geometry using a Cu $K\alpha$ radiation. The incidence angle was 0.5° which corresponds to a penetration depth of approximately 250 nm. Fe concentration profiles were measured by 2.2-MeV $^4He^+$ Rutherford backscattering spectrometry (RBS). These data were analyzed using the RUMP code.[22]

Magnetic measurements were performed using a superconducting quantum interference device (SQUID) magnetometer and a vibrating-sample magnetometer. Hysteresis loops were measured at 3 K and 77 K applying the magnetic field parallel to the film surface. Zero-field-cooled (ZFC) magnetization measurements were realized by applying a magnetic field of 5 mT and increasing the temperature from 3 K up to room temperature. The field-cooled (FC) magnetizations were measured cooling the sample down to 3 K in the fixed magnetic field of the same value as mentioned above.

B. Electrical measurements

Studying the electrical transport in a thin-film Fe-Ta-O nanocomposite[23] we found it reasonable to reduce the volume of the sample to be probed by a current in order to address only a few nanoparticles in the nanocomposite. Therefore, we developed a procedure for the fabrication of post-deposited planar electrodes with a gap of only 100 nm or less, using just optical photolithography and electromigration effects. Since in the as-prepared sample the Fe-SiO_2 nanocomposite layer was buried in a silica substrate [Fig. 1(a)] in fact, electrically insulated by a top layer of silica in which no nanoparticles were formed due to relatively high

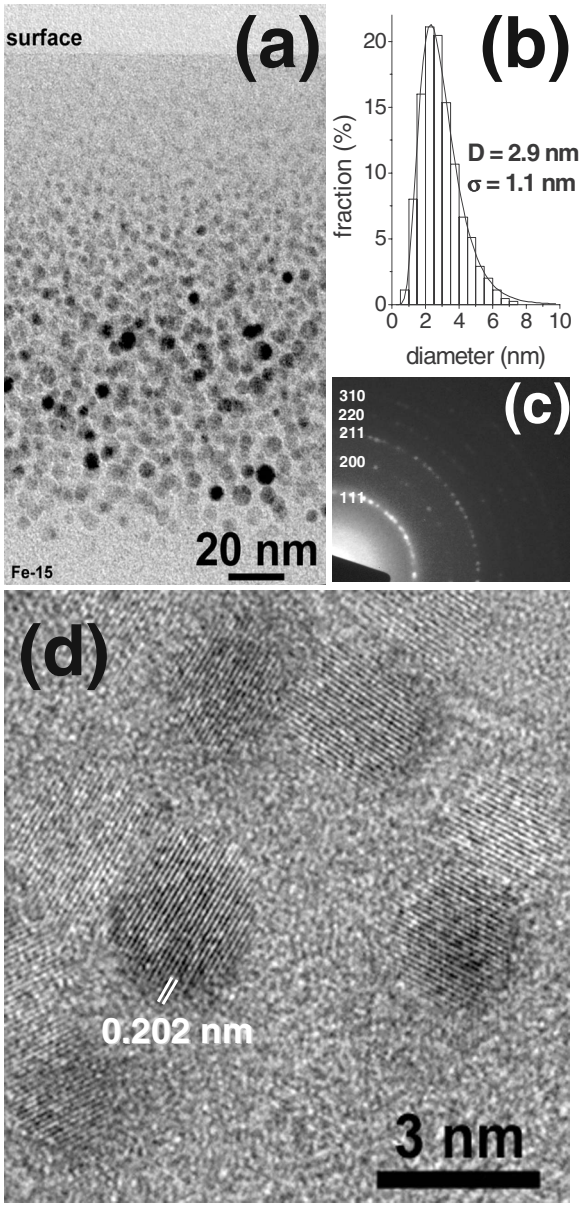

FIG. 1. (a) Cross-sectional bright-field TEM micrograph of the Fe-SiO_2 composite, (b) corresponding particle-size distribution, (c) SAED pattern with indices corresponding to the bcc structure of Fe, and (d) high-resolution TEM micrograph of the Fe-SiO_2 sample.

implantation energy, it was at first necessary to cautiously remove a thin layer of silica (~70 nm) by Ar-ion plasma etching from the top of the sample. Then a gold layer, ~100 nm thick (with a thin Ti adhesion sublayer deposited first), was evaporated on this surface. Using a conventional optical photolithography, 110 "short-circuited" four-terminal patterns were patterned on the as-implanted specimen of 1 $\times 1$ cm^2 size [Fig. 2(a)], which were then used as a self-aligned mask. The dry etching was stopped just after a mesa structure was patterned [Fig. 2(b)], i.e., the Fe-SiO_2 nanocomposite was present only beneath the gold four-terminal pattern.

As the next step, the narrowest part in the middle of the pattern (2 μm wide and 2 μm long stripe) was open cir-

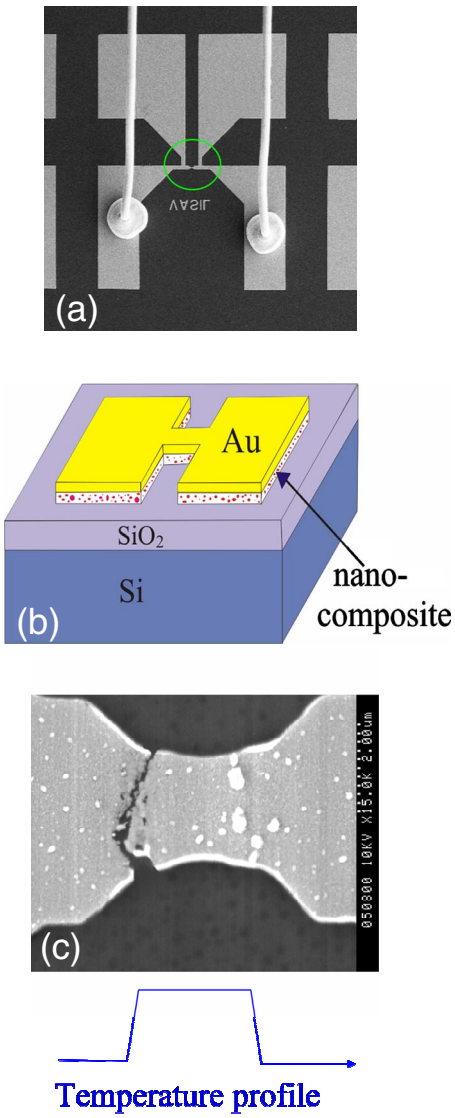

FIG. 2. (Color online) (a) SEM view of the four-probe pattern, (b) sketch of the single pattern showing the mesa structure, before opening the top gold layer by electromigration, and (c) the gold strip open circuited by electromigration and the corresponding temperature profile along the stripe.

cuited by electromigration at room temperature in about 40–50 min. The initial current of about 25 mA (which corresponded to a current density of about 5×10^6 A/cm^2) was supplied from a constant-voltage (CV) source. The electromigration was performed in a scanning electron microscope for two reasons: to control the process visually and to benefit from vacuum environment, which provided a more suitable temperature profile along the gold stripe than an air environment. The temperature profile with high gradients is a consequence of (i) intensive Joule heating of the stripe due to a very high current density in it and (ii) a high cooling rate of the large-area contact pads. A high-temperature gradient plays an important role in the mass flow of gold atoms within the gold stripe.[24,25] According to our experience, the CV regime is more suitable than the constant-current supply, because in the latter case, the current density steeply increases in a final stage of the electromigration process and the already thinned (depleted) region of a gold strip could blow up as a fuse, which results in a wide gap. Moreover, the CV supply ensures that in the moment of the formation of the gap, the electric field is kept low. This avoids irreversible changes in nanocomposites, which could be caused by the application of high electric fields[26] and an abrupt temperature rise in the final stage.

The result of the electromigration process was the formation of the gap in the gold layer less than 100 nm wide, situated closer to one of the electrodes, depending on the polarity of the electromigration current [Fig. 2(c)]. The estimated volume of the nanocomposites, probed by a current during the transport measurements, is about $100\times2000\times100$ nm^3.

In some sense, our technique used for the preparation of the electrodes is similar to the granular-in-gap technique,[4] but in the latter case the electrodes must be prepared prior the deposition of a nanocomposite. In some cases this could cause a problem, because no nanoparticles are formed in the very vicinity of the electrodes which hinders the tunneling current. This happens when a relatively thin nanocomposite layer is deposited by the evaporation or sputtering on relatively thick predeposited electrodes.[27] On the other hand, our procedure has a limitation as well—it is applicable only to nanocomposites with sufficient resistance (in practice, to those with an insulating matrix).

The resistivity and *I-V* curves were measured by a HP picoammeter/dc voltage source in a temperature range of 4.2–300 K. The magnetoresistivity was measured at 77 K in magnetic field up to 1.2 T. Since the sample resistivities were of the order of 10^8–10^{10} Ω, a two-terminal configuration was sufficient for accurate measurements of $R(T)$, *I-V*, and $R(B)$ dependences. The measurements were performed in vacuum.

III. RESULTS AND DISCUSSION

A. Structural characterization

Figure 1(a) shows a cross-sectional bright-field TEM micrograph of the sample, and Fig. 1(b) shows the corresponding histogram of the nanoparticle size distribution. Spherical nanoparticles are dispersed in the silica glass, most of them being distributed in a sublayer of ~100 nm thick, the center of which is ~110 nm beneath the surface. The nanoparticles have an average size of 2.9 nm with a standard deviation of 1.1 nm. The SAED pattern [Fig. 1(c)] shows the presence of a single-crystalline bcc structure with a lattice parameter equal to 0.286±0.001 nm which is comparable to that of bulk Fe (0.285 70 nm). No evidence of oxide (crystalline or amorphous) nanoparticles was obtained from high-resolution SAED or GIXRD measurements. Moreover, the high-resolution TEM micrographs [Fig. 1(d)] do not show the presence of an oxide shell around the nanoparticles.

The analysis of the RBS data shows that in the implanted region the Fe peak concentration corresponds to a metal/SiO_2 ratio of around 0.8. Considering the limiting case that all implanted Fe atoms are included in metal nanoparticles, the above-mentioned ratio corresponds to an average maximum volumetric Fe concentration (filling factor) of approximately

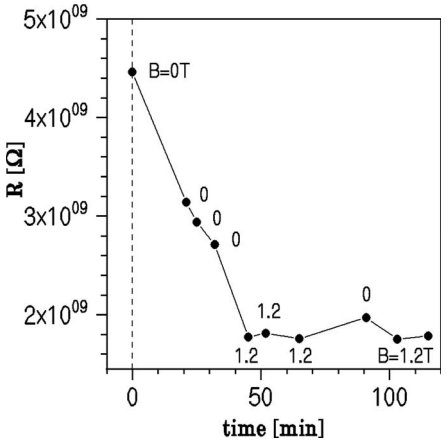

FIG. 3. Time dependence of the composite resistivity determined from *I-V* curves as dI/dV against bias voltage plots at $V=0$. In some cases a parallel magnetic field of 1.2 T was applied.

0.14 which corresponds to an average center-to-center distance of about 5 nm taking into account the average particle size estimated from TEM. This value is below the physical percolation limit, so the nanoparticles do not touch each other, as can be seen in Fig. 1(a).

B. Electrical transport in the nanocomposite

Since the matrix material is an insulator and the interparticle distance estimated from RBS data is about 2–3 nm, it is obvious that the prevailing mechanism of electrical transport is the tunneling of electrons between the adjacent iron nanoparticles through a silica barrier. About 20 of the 110 four-probe patterns were open circuited by electromigration. We found that not all of these 20 samples exhibited single-electron phenomena. Usually, we measured a set of *I-V* curves at various temperatures from 4 to 300 K. The measurements performed repeatedly at the same temperature showed an interesting feature of the nanocomposite system: several-minutes-lasting formation of a "steady" tunneling conduction path. This is evidenced in Fig. 3 showing a time dependence of the sample resistance at 77 K that underwent a repeated bias-voltage sweep in a range of 1 V. As can be seen, the resistance (calculated from dI/dV vs V curves at $V=0$) decreased with time to one-third of its initial value independent of whether a magnetic field of 1.2 T was applied or not. Once the optimal tunneling path was established, the *I-V* curves were more or less reproducible.

Almost all the samples showed strongly nonlinear *I-V* curves even at room temperature. A typical curve is depicted in Fig. 4(a). Some samples showed rectifying behavior—asymmetric *I-V* curves resembling diode characteristics [Fig. 4(b)]—but after several voltage sweeps this feature disappeared and the *I-V* curves became symmetric and nonlinear. Below ~70 K and above a threshold voltage V_T ~220 mV, the *I-V* curves follow approximately a dependence $I \sim (V-V_T)$,[3] which is typical for elastic tunneling in conventional tunneling junctions.

The most interesting *I-V* curves were obtained with one of the 20 circuits at 4.2 K; one of them is shown in Fig. 5(a).

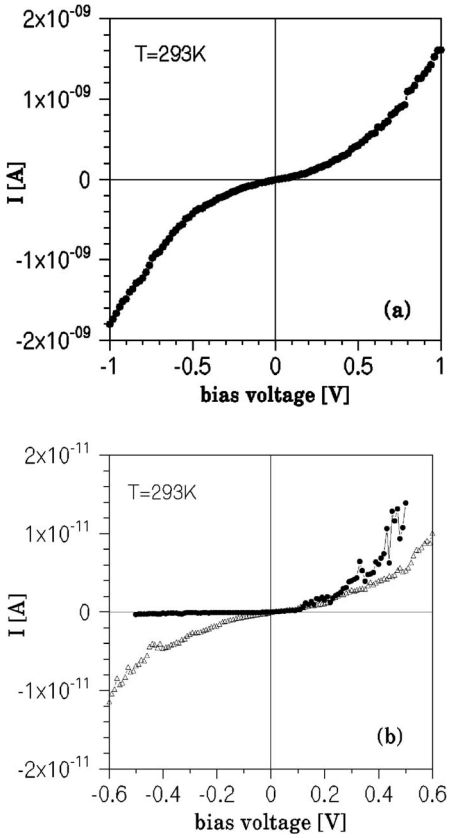

FIG. 4. (a) A typical nonlinear *I-V* curve measured at room temperature and (b) some samples exhibiting a rectifying behavior (solid circles) that disappeared after several voltage sweeps (open triangles).

Especially at negative bias [Fig. 5(b)], one sharp and several rounded steps are clearly visible. This is the well-known single-electron transport phenomenon called Coulomb staircase.[2,3] This fact has several implications: somewhere in the volume of the nanocomposite probed by the current a random quasi-one-dimensional (quasi-1D) chain of iron nanoparticles separated from each other by silica tunneling barriers must be set up.[28] Though this chain has the lowest resistance from all the other possible chains, it must include a "bottleneck"—a double junction that governs the transport (see Fig. 6). The double junction must be strongly asymmetric—i.e., $R_1C_1 \gg R_2C_2$ (R_i and C_i being the effective resistance and capacitance of the corresponding junction) and, simultaneously, $R_i > R_Q$ ($R_Q=h/2e^2$ is the resistance quantum) to avoid quantum fluctuations. Moreover, the charging energy $E_c=e^2/2C$ must be much larger than k_BT, in order to avoid thermal fluctuations. The asymmetry in the electronic direction is a consequence of the geometrical asymmetry: a possible arrangement could be that in a row of three adjacent nanoparticles, the middle one (and the smallest one with the largest E_c) is placed asymmetrically between the other two. We can readily estimate how many nanoparticles should be contained in a straight chain between the planar electrodes. The result is 17–20 nanoparticles, supposing an average size of the nanoparticles of 2.9 nm, interparticle distance 2–3 nm, and separation of electrodes 100 nm. Actually, the number of particles in the chain could be even

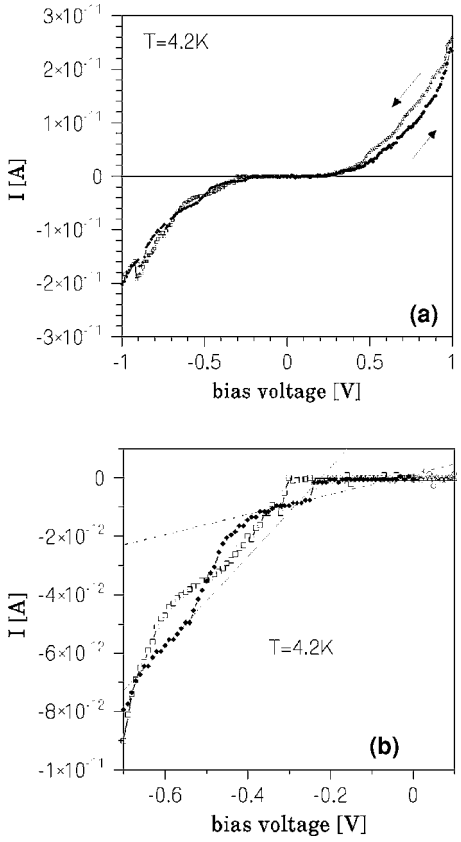

FIG. 5. (a) Steps in the *I-V* curve measured at 4.2 K and (b) detail of the same curve at negative bias.

smaller, since after a thorough inspection of the scanning tunneling microscope (SEM) micrograph, shown in Fig. 2(c), it was found that the edges of the gap were not straight but meandering, so at some places the gap was only 20 nm wide. The self-selection process of an optimal tunneling path is described in Ref. 28, where it is also pointed out that the remaining tunnel junctions in series with the double junction play an important role in the isolation of the controlling nanoparticle from its environment, thus stabilizing its charge states for a reasonable period of time, which makes it easier to observe the single-electron phenomena.

In order to better reveal the steps, the curve shown in Fig. 5(a) was differentiated and plotted against the bias voltage in Fig. 7. As can be seen, the current steps occur regularly with a period in voltage $\Delta V = e/C$ of about 220 mV. From this value one can calculate the capacitance C of the nanoparticle that governs the transport to be $C \sim 7 \times 10^{-19}$ F. Applying the formula for the calculation of the self-capacitance of a sphere, $C = 4\pi\varepsilon_0\varepsilon_r R$, and supposing a value of ε_r of SiO_2

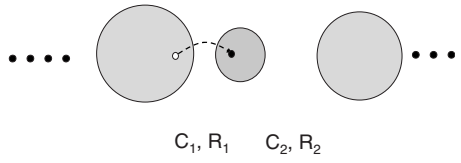

FIG. 6. Schematic illustration of a double junction governing the transport in a random quasi-1D chain of several Fe nanograins.

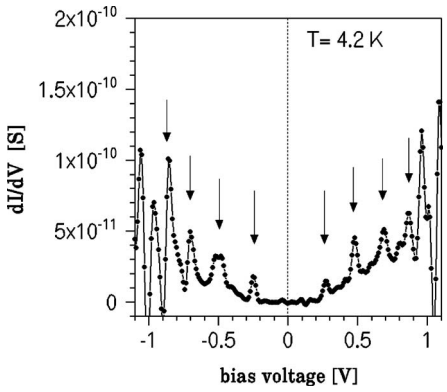

FIG. 7. Differential conductivity plotted against bias voltage depicts more clearly the steps in the *I-V* curve shown in Fig. 5(a).

equal to 4 (Ref. 29), one obtains a diameter of the nanoparticle $2R = 3.1$ nm, which corresponds well to the mean size of 2.9 nm obtained from analysis of the TEM micrographs [Fig. 1(b)].

We have observed that each successive *I-V* curve was a bit different compared to previous one, and after several hours of repeated *I-V* measurements the Coulomb staircase disappeared. In Fig. 5(b) it can be seen that even during the measurement of the same *I-V* curve the steps were shifted by ~ -60 mV as the bias voltage decreases. Similar behavior was reported for a gold/polymer nanocomposite by Berven *et al.* in Ref. 30. This effect can be attributed to slow fluctuations in a background charge and is encountered also in conventional single-electron devices where it causes a serious problem. The gradual disappearance of the rectifying behavior [Fig. 4(b)] is also explainable by the background charge fluctuations.[31] The role of the background charge is illustrated in Fig. 18 in Ref. 3. So we can conclude that in our sample the role of an external gate was played by a randomly charged nanoparticle(s) situated in the vicinity of the self-selected tunneling path.

According to Ref. 28 the transport in a metal/insulator nanocomposite is a mixture of (i) direct tunneling, (ii) resonant tunneling via localized centres, and (iii) thermally activated jumps. This probably explains why the slope of the "plateau" in the current steps [Fig. 5(b)] increases with the increasing bias voltage. The slope of the first step corresponds to $R = 2.9 \times 10^{11}$ Ω, but the slope of the second step indicates a differential resistance of only 0.66×10^{11} Ω. Presumably, this increase in conductivity is caused by the opening of additional conduction paths with increasing bias.

Around zero bias voltage, the Coulomb blockade of tunneling was noticeable up to $T \sim 55$ K. We also measured $R(B)$ dependences in parallel and perpendicular fields up to 1.2 T at room temperature and 77 K, expecting to observe negative tunneling magnetoresistivity.[32] The resistance of our samples was, however, independent of magnetic field even at 77 K. The reason could be that the ion implantation technique provides nanoparticles that are too small. In this respect, it is worth mentioning that Mitani *et al.*[32] reported on relatively high TMR values of almost 40% observed in a Co-Al-O nanocomposite. The study also indicates some synergetic effect of the Coulomb blockade and spin-dependent

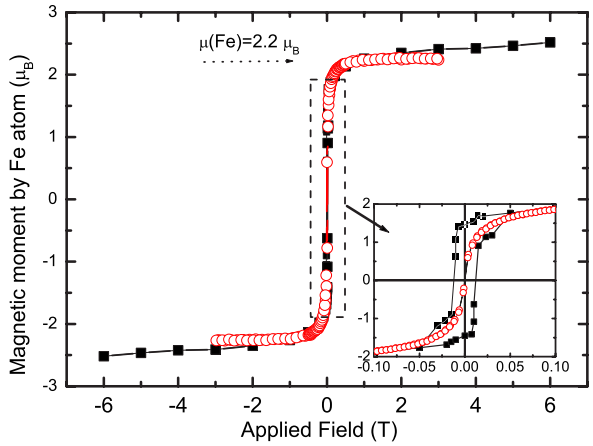

FIG. 8. (Color online) Hysteresis loops measured at 4 K (solid square symbols) and 77 K (circle symbols). Inset: detail of the loops in the low-magnetic-field region.

tunneling. Unfortunately, the authors do not provide any direct evidence of the magnetoresistivity, since their TMR values are obtained just by a subtraction of two *I-V* curves measured with and without an external magnetic field. The point is that such a procedure could be misleading due to the fluctuations of background charge in a nanocomposites, as is discussed above. Referring to our cyclic measurements of *I-V* curves summarized in Fig. 3 as $R(V=0)$ versus time plot with an external field as the parameter, we could obtain both positive and negative magnetoresistivity derived from subtraction of the successive *I-V* curves. In our opinion direct $R(B)$ measurements are inevitable for evidencing magnetoresistivity in metal/insulator nanocomposites.

C. Magnetic properties

In order to elucidate the absence of the negative magnetoresistivity we examined the magnetic properties of the nanocomposite. At first, we measured the hysteresis loops at 3 K and 77 K. The data were corrected by subtracting the diamagnetic contribution of the silica substrate which had been independently measured in pure silica slides. Figure 8 represents both hysteresis loops in which the magnetization is represented in terms of normalized magnetic moment per Fe atom. This was calculated considering the implanted fluence obtained from RBS measurements. At 3 K the magnetization does not saturate at the largest magnetic field and the Fe magnetic moment $[(2.5\pm0.2)\mu_B$ at 6 T] is larger than the bulk α-Fe value $(2.2\mu_B)$. However, at 77 K and above the field of 1.5 T, the magnetization reaches a smaller saturated value of $(2.3\pm0.2)\mu_B$. Both the nonsaturation of the magnetization at high field and the large magnetic moment of the Fe nanoparticles could be related to the magnetic contribution of free paramagnetic ions, but also to the magnetic behavior of Fe-oxide nanoparticles,[33–36] which presents magnetic frustration of the antiferromagnetic order on their surfaces. It is supposable that the surfaces of the nanoparticles are oxidized, giving rise to a core-shell structure. In our case, neither high-resolution TEM nor GIXRD studies indicated the presence of crystalline oxides or oxide shells surrounding the metallic nanoparticles. On the other hand, the presence of a small quantity of oxidized Fe ions cannot be ruled out purely from the structural point of view. Mössbauer studies by Perez *et al.*[15] have shown the presence of various ions and oxides in Fe-implanted silica, the amount of which decreases as the implanted dose increases. It means that in the sample some paramagnetic Fe atoms or oxide clusters could be present considering the nonsaturation of magnetization measured at 4 K. In both species one could expect a decrease in the magnetic moment as the temperature increases. In the case of paramagnetic ions the magnetization follows Curie's law while the iron oxide clusters should show reduced Néel temperatures. For example, we can assume that the difference in magnetizations obtained in the field of 6 T at 4 K and 77 K $(0.3\mu_B)$ is due to the presence of the free atoms in the most oxidized state, Fe^{3+}, with an effective magnetic moment of $5.9\mu_B$. Thus, the estimated percentage of free Fe atoms is around 8%. However the field dependence of the magnetization, calculated using a Langevin function, of Fe^{3+} does not show a linear dependence at low temperature of 4 K and it is almost saturated above the magnetic field of 1 T. This is in contradiction to the observed susceptibility at high field, and we could conclude that the magnetic moment of the possible paramagnetic species is smaller than that of free ions. We could try to obtain such information analyzing the magnetic moment of Fe metallic clusters. The calculated value of magnetic moment per atom of metallic Fe at 77 K is larger than that of bulk iron. Several studies[37–41] have shown this increase in Fe clusters which is associated with an enhanced orbital magnetic moment produced by modification of the electronic structure at the nanoparticle surface. The magnetic moment of free clusters is size dependent, evolving from around $3\mu_B$/atom to the bulk value as the size increases from 1 to 3 nm.[38,41] Considering that the nanoparticles in the nanocomposite have sizes from 1 to 6 nm, only a fraction of these should exhibit such an enhancement of magnetization. We point out that these values correspond to the free clusters and not to the clusters embedded in a matrix (our case), in which the electronic structure and also the magnetic moment are different. Then estimation of the nature and quantity of these compounds (ions, oxide clusters, or Fe nanoparticles) is not possible. However, the fact that the magnetic moment reaches almost the bulk value and considering the result by Perez *et al.*[15] that the fraction of nonmetallic compounds is quite reduced for doses larger than 10^{17} Fe^+/cm^2 implies that the percentage of metallic Fe nanoparticles is dominating over the nonmetallic compounds.

The inset of Fig. 8 shows a detail of the hysteresis loops at low magnetic fields. It can be observed that the hysteresis loop at 3 K is open and the coercive field is 15 ± 2 mT, while at 77 K, the magnetization versus magnetic field does not show any hysteresis. This decrease in coercivity with increasing temperature is usually attributed to a progressive increase in the number of superparamagnetic nanoparticles.[8,9,42] In order to investigate this effect, ZFC and FC magnetization measurements were performed and the results are represented in Fig. 9. ZFC magnetizations show a maximum at $\langle T_B \rangle = 41$ K and the ZFC and FC curves join together at the temperature $T_{Bmax}=170$ K. These data suggest

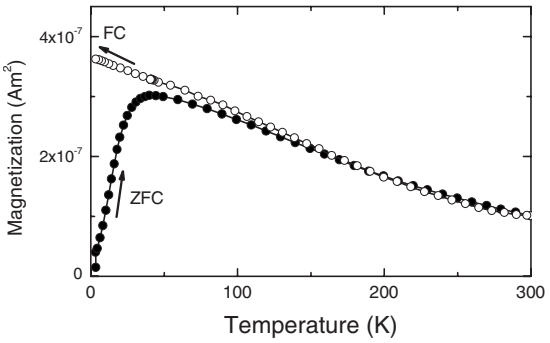

FIG. 9. Temperature dependence of the ZFC and FC magnetization measurements.

that the composite exhibited a blocking-temperature distribution which can be represented by the average blocking temperature $\langle T_B \rangle$,[8,42] while above T_{Bmax} all the nanoparticles were superparamagnetic. This broad blocking-temperature distribution is probably associated with the particle-size distribution. In order to better understand these results, the ZFC-FC magnetization curves were calculated considering the Arrhenius model of superparamagnetism, the measured particle size distribution, and a constant value of the magnetic anisotropy, K_{eff}, as described in Refs. 42 and 43. The best fit was obtained using a value of $K_{eff}=2\times10^5$ J m^{-3}. This value is huge in comparison with the bulk magnetocrystalline anisotropy of Fe (4.8×10^4 Jm^{-3}), and it must be due to the contribution of the surface.[9,40]

As mentioned above, the ZFC-FC curves became identical above 170 K, which indicates that below this temperature both the superparamagnetic and blocked nanoparticles were present in the nanocomposite. Normally, a nonzero coercive field is clear evidence that nanoparticles are blocked. However, at 77 K the hysteresis loop does not show any coercive field or remanent magnetization while the ZFC-FC curves do not coincide. In this discussion we have assumed that the energy barrier characteristics of the nanoparticles are equal in both types of measurements. This is not true if interparticle interactions are present. Even if the volumetric concentration of nanoparticles is small, the large magnetic moment of Fe and its characteristic low magnetic anisotropy may cause the interparticle interactions to play an important role in both the thermal-driven (superparamagnetism) and the magnetostatic-driven (hysteresis) demagnetization processes. In fact, the magnetization curves at temperatures above T_B ($T>200$ K) follow the Curie-Weiss law with $M(T) \propto M_0/(T-T_0)$ where M_0 is a constant and T_0 is the Curie-Weiss temperature. The T_0 value is related to the effect of the dipolar interactions in a weak-coupling regime[42,44] which is characteristic of diluted materials. In our measurements the obtained T_0 is +60 K, indicating that dipolar interparticle interactions produce ferromagneticlike coupled structures.

Finally, we should discuss why no tunneling magnetoresistivity was observed in our Fe-SiO_2 composite. From the morphological point of view, the composite contains separated crystalline Fe nanoparticles with magnetic properties similar to those expected in ferromagnetic nanogranular materials: enhanced magnetic moment and anisotropy due to surface effects in the nanoparticles and weak interparticle coupling. However, magnetotransport was not observed though in similar nanocomposites prepared by ion implantation—e.g., Fe-Al_2O_3. Sakamoto *et al.*[16] reported TMR values up to 8.5% at room temperature, and Hayashi *et al.*[17] reported TMR=7.5%, obtained in the Fe-Co-Al_2O_3 system. But in both studies the resulting metal concentration was larger than in our case because of the higher implanted fluences and lower implantation energy. Moreover, our samples were not annealed after implantation which implies a higher number of single Fe atoms present in the tunneling barrier (silica). It is well known that such atoms are efficient magnetic scatterers and can cause spin flips during the tunneling event which substantially reduces the TMR value.

IV. CONCLUSIONS

An Fe-SiO_2 nanocomposite was prepared by ion implantation. In order to measure its transport properties in a limited volume of almost nanoscale dimensions, special gold thin-film electrodes were fabricated by using a conventional photolithography and electromigration. The single-electron transport phenomena were observed at 4 K, a Coulomb blockade with threshold voltage of 220 mV and a Coulomb staircase with equidistant steps in voltage. The presence of Coulomb steps in *I-V* curves implies that the electric transport is accomplished by tunneling of electrons one by one via a random quasi-1D chain consisting of only a few isolated iron nanoparticles. The transport characteristics evolve with time due to fluctuations in background charge present in the vicinity of the tunneling path. However, even if nanostructural and magnetic properties show the presence of ferromagnetic Fe nanoparticles isolated in SiO_2, magnetoresistivity at 77 K is not observed. This effect is attributed to the low concentration of the nanoparticles and the spin-flip contribution of the single Fe atoms present in the matrix.

ACKNOWLEDGMENTS

This work was initiated thanks to the workshop held in Leuven in 2002 and organized by COST Action 523 on Nanostructured materials. V. Smatko and E. Kovacova are thanked for patterning the electrodes. I. Kostic at the II SAS in Bratislava is acknowledged for the SEM micrographs. C. Battaglin is thanked for the RBS measurements. This work was financially supported by FIRB "Micropolys" and COFIN Italian projects, by CNR-SAV bilateral project, and VEGA project No. 2/3119/25.

*Electronic address: eleklobo@savba.sk

[1] *Single Charge Tunneling*, edited by H. Grabert and M. H. Devoret (Plenum Press, New York, 1999).
[2] *Mesoscopic Electronics in Solid State Nanostructures*, edited by T. T. Heinzel (Willey-VCJ, Weinheim, 2003).
[3] K. K. Likharev, Proc. IEEE **87**, 606 (1999).
[4] H. Fujimori, S. Mitani, and K. Takanashi, Mater. Sci. Eng., A **267**, 184 (1999).
[5] M. Julliere, Phys. Lett. **54**, 225 (1975).
[6] J. S. Moodera, L. R. Kinder, T. M. Wong, and R. Meservey, Phys. Rev. Lett. **74**, 3273 (1995).
[7] C. L. Chien, J. Q. Xiao, and J. S. Jiang, J. Appl. Phys. **73**, 5309 (1993).
[8] J. L. Dormann, D. Fiorani, and E. Tronc, Adv. Chem. Phys. **98**, 283 (1997).
[9] X. Batlle and A. Labarta, J. Phys. D **35**, R15 (2002).
[10] S. Honda, T. Okada, M. Nawate, and M. Tokumoto, Phys. Rev. B **56**, 14566 (1997).
[11] B. Dieny, S. Sankar, M. R. McCartney, D. J. Smith, P. Bayle-Guillemaud, and A. E. Berkowitz, J. Magn. Magn. Mater. **185**, 283 (1997).
[12] M. Anas, C. Bellouard, and M. Vergnat, J. Appl. Phys. **88**, 6075 (2000).
[13] N. M. Dempsey, L. Ranno, D. Givord, J. Gonzalo, R. Serna, G. T. Fei, A. K. Petforf-Long, R. G. Doole, and D. E. Hole, J. Appl. Phys. **90**, 6268 (2001).
[14] P. Lobotka, I. Vávra, F. Fendrych, and L. Kraus, J. Magn. Magn. Mater. **240**, 491 (2002).
[15] A. Perez, M. Treilleux, T. Capra, and D. L. Griscom, J. Mater. Res. **2**, 910 (1987).
[16] I. Sakamoto, S. Honda, H. Tanoue, N. Hayashi, and H. Yamane, Nucl. Instrum. Methods Phys. Res. B **148**, 1039 (1999).
[17] N. Hayashi, I. Sakamoto, H. Wakabayashi, T. Toriyama, and S. Honda, J. Appl. Phys. **94**, 2597 (2003).
[18] T. Moriwaki, H. Hayashi, I. Sakamoto, H. Tanoue, T. Toriyama, and H. Wakabayashi, Trans. Mater. Res. Soc. Jpn. **29**, 607 (2004).
[19] F. Gonella and P. Mazzoldi, in *Handbook of Nanostructured Materials and Nanotechnology*, edited by H. Singh Nalwa (Academic Press, San Diego, 2000), Vol. 4, p. 81.
[20] A. Meldrum, R. F. Haglund Jr., L. A. Boatner, and C. W. White, Adv. Mater. (Weinheim, Ger.) **13**, 1431 (2001).
[21] G. Mattei, Nucl. Instrum. Methods Phys. Res. B **191**, 323 (2002).
[22] L. R. Doolittle, Nucl. Instrum. Methods Phys. Res. B **9**, 344 (1985).
[23] P. Lobotka, I. Vávra, F. Fendrych, and S. Chayka, Phys. Status Solidi A **201**, 1493 (2004).
[24] I. Vávra, P. Lobotka, F. Zachar, and J. Osvald, Phys. Status Solidi A **63**, 363 (1981).
[25] P. Lobotka and I. Vávra, Phys. Status Solidi A **63**, 655 (1981).
[26] R. D. Fedorovich, Phys. Rep. **328**, 73 (2000).
[27] S. Gazi (unpublished), results obtained from experiments with NbN/AlN nanocomposite system prepared by sequential sputtering on a substrate with pre-patterned NbN electrodes 100 nm thick.
[28] S. V. Vyshenski, JETP Lett. **61**, 111 (1995).
[29] *CRC Handbook of Chemistry and Physics*, 51st ed. (CRC, Cleveland, 1971).
[30] C. A. Berven, M. N. Wybourne, L. Clarke, L. Longstreth, J. E. Hutchison, and J. L. Mooster, J. Appl. Phys. **92**, 4513 (2002).
[31] M. Stopa, Phys. Rev. Lett. **88**, 146802 (2002).
[32] S. Mitani, K. Takanashi, K. Yakushiji, J. Chiba, and H. Fujimori, Mater. Sci. Eng., B **84**, 120 (2001).
[33] J. M. D. Coey, Phys. Rev. Lett. **27**, 1140 (1971).
[34] A. H. Morrish and K. Haneda, J. Magn. Magn. Mater. **35**, 105 (1983).
[35] M. P. Morales, S. Veintemillas-Verdaguer, M. I. Montero, C. J. Serna, A. Roig, Ll. Casas, B. Martínez, and F. Sandiumenge, Chem. Mater. **11**, 3058 (1999).
[36] S. Mørup, J. Magn. Magn. Mater. **266**, 110 (2003).
[37] U. Herr, J. Ring, R. Birringer, U. Gonser, and H. Gleiter, Appl. Phys. Lett. **50**, 472 (1987).
[38] I. M. L. Billas, J. A. Becker, A. Châtelain, and W. A. de Heer, Phys. Rev. Lett. **71**, 4067 (1993).
[39] K. W. Edmonds, C. Binns, S. H. Baker, S. C. Thornton, C. Norris, J. B. Goedkoop, M. Finazzi, and N. B. Brookes, Phys. Rev. B **60**, 472 (1999).
[40] J. Bansmann, S. H. Baker, C. Binns, J. A. Blackman, J.-P. Bucher, J. Dorantes-Dávila, V. Dupuis, L. Favre, D. Kechrakos, A. Kleibert, K.-H. Meiwes-Broer, G. M. Pastor, A. Perez, O. Toulemonde, K. N. Trohidou, J. Tuaillon, and Y. Xiec, Surf. Sci. Rep. **56**, 189 (2005).
[41] M. L. Tiago, Y. Zhou, M. M. G. Alemany, Y. Saad, and J. R. Chelikowsky, Phys. Rev. Lett. **97**, 147201 (2006).
[42] M. El-Hilo, K. O'Grady, and R. W. Chantrell, J. Magn. Magn. Mater. **114**, 295 (1992).
[43] C. de Julián Fernández, Phys. Rev. B **72**, 054438 (2005).
[44] R. W. Chantrell and E. P. Wohlfarth, J. Magn. Magn. Mater. **40**, 1 (1983).